



**HAL**  
open science

## Energy management of a thermally coupled fuel cell system and metal hydride tank

Djafar Chabane, Mona Ibrahim, Fabien Harel, Abdesslem Djerdir, Denis Candusso, Omar Elkedim

► **To cite this version:**

Djafar Chabane, Mona Ibrahim, Fabien Harel, Abdesslem Djerdir, Denis Candusso, et al.. Energy management of a thermally coupled fuel cell system and metal hydride tank. *International Journal of Hydrogen Energy*, 2019, 44 (50), pp.27553-27563. 10.1016/j.ijhydene.2019.08.247 . hal-02311605

**HAL Id: hal-02311605**

**<https://hal.science/hal-02311605v1>**

Submitted on 20 Jul 2022

**HAL** is a multi-disciplinary open access archive for the deposit and dissemination of scientific research documents, whether they are published or not. The documents may come from teaching and research institutions in France or abroad, or from public or private research centers.

L'archive ouverte pluridisciplinaire **HAL**, est destinée au dépôt et à la diffusion de documents scientifiques de niveau recherche, publiés ou non, émanant des établissements d'enseignement et de recherche français ou étrangers, des laboratoires publics ou privés.



Distributed under a Creative Commons Attribution - NonCommercial 4.0 International License

# Energy management of a thermally coupled fuel cell system and metal hydride tank

D.Chabane<sup>a,b,\*</sup>, M.Ibrahim<sup>c</sup>, F.Harel<sup>d</sup>, A.Djerdir<sup>a,b</sup>, D. Candusso<sup>e</sup>, O.Elkedim<sup>a,f</sup>

<sup>a</sup>*FEMTO-ST, CNRS, Univ. Bourgogne Franche-Comté, UTBM*

<sup>b</sup>*FCLAB, CNRS, Univ. Bourgogne Franche-Comte Rue Thierry Mieg, F-90010 Belfort Cedex, France*

<sup>c</sup>*University of Surrey, department of physics, GU2 7XH, Guildford, UK*

<sup>d</sup>*IFSTTAR / AME / LTE, 25 avenue François Mitterrand, Case 24, Cité des mobilités, F-69675 Bron cedex, France.*

<sup>e</sup>*IFSTTAR / COSYS / SATIE (UMR CNRS 8029), 25 allée des marronniers, 78000 Versailles Satory, France*

<sup>f</sup>*FEMTO-ST, MN2S, Université de Bourgogne Franche-Comté, Site de Sévenans, 90010 Belfort cedex, France*

---

## Abstract

Being produced from renewable energy, hydrogen is one of the most efficient energy carriers of the future. Using metal alloys, hydrogen can be stored and transported at a low cost, in a safe and effective manner. However, most metals react with hydrogen to form a compound called metal hydride (MH). This reaction is an exothermic process, and as a result releases heat. With sufficient heat supply, hydrogen can be released from the as-formed metal hydride. In this work, we propose an integrated power system of a proton exchange membrane fuel cell (PEMFC) together with a hydride tank designed for vehicle use. We investigate different aspects for developing metal hydride tanks and their integration in the PEMFC, using water as the thermal fluid and a FeTi intermetallic compound as the hydrogen storage material. Ground truth simulations show that the annular metal hydride tank meets the hydrogen requirements of the fuel cell, but to the detriment of the operating temperature of the fuel cell (FC).

*Keywords:* Fuel cell, Energy management, Hydrogen tank, thermal coupling

---

## 1. Introduction

Integrated systems composed of a PEMFC stack and metal hydride tanks have been widely studied by researchers. Systems where the wasted heat generated in the fuel cell is used to supply the heat required for desorption of hydrogen from the tank have been investigated in [1–12]. Different modes of heat transfer such as direct [8], air [2], heat transfer fluid [13] and heat pipes [10] are used to carry out the coupling. An important work

---

\*Corresponding author

Email address: [djafar.chabane@utbm.fr](mailto:djafar.chabane@utbm.fr) (D.Chabane)

in [8] considers high and low temperature of the FC. The authors suggest a direct transfer of calories from the FC to the hydride tank for high temperature fuel cell. The calorific power of the solid-oxide fuel cell (SOFC) is transferred mainly by radiation, convection, and conduction to the hydride tank. As for low temperature FC, such as PEMFC, the authors suggest an indirect transfer based on passive or active thermal bridges to transfer calories from the FC to the storage system.

In [10], the authors propose a technology based on the use of passive bridges (heat pipes) to minimize the dissipated thermal energy encountered in the active cooling technique. In order to achieve a better heat transfer, a new system is proposed by Zhixiang et al. in [9], which consists of directly integrate the hydrogen storage into the FC. This technology allows a direct transfer of heat from the battery to the hydride tank.

In [14], Weiss et al. study a HT-PEM fuel cell stack (400 W) coupled to a sodium alanate storage tank (300 g material). This study shows that the amount of heat produced by the fuel cell stack is sufficient to desorb the necessary amount of hydrogen from the storage tank. Furthermore, they demonstrate that the reaction rate of the sodium alanate required to provide the hydrogen to the fuel cell stack was reached for a temperature of  $160^{\circ}\text{C}$  and for a pressure of 1.7 [bar].

Some other important studies considering active systems are suggested in [13, 15]. The authors propose the use of heat exchangers for embedded and stationary applications.

Several simulation works have also shown important results for coupling and heat transfer. For instance, Pfeifer et al. in [3] simulate the heat of a high temperature PEM fuel cell and an alanate hydrogen storage tank by using the software package gPROMS. The results show that the initial temperature has a considerable influence on the operation time, due to the possible break-down of hydrogen pressure in the tank. The simulation has been validated with a small tank.

The authors in [16] presented a new design of a MH hydrogen storage tank for fuel cell utility vehicles. This solution consists in stacking several MH cassettes each comprising several MH containers made of stainless steel tube with embedded (pressed-in) perforated copper fins and filled with a powder of a composite MH material which contains AB2- and AB5-type hydride forming alloys and expanded natural graphite. This new design offers many advantages such as adjustable high weight, compactness and a good dynamics of hydrogen charge/discharge.

Another application of hydrogen storage as a solid form is presented in [17]. They developed a high temperature Metal Hydride Water Pumping System (MHWPS) equipped with a latent heat exchanger. The operating concept of the pump and the mathematical model translating the heat and mass transfer within the pump was established. The simulation results shown an improvement of the dynamic behavior of the system, a reduction in the pumping time of about 90% and an increase of the efficiency of the pump of about 7.6 times.

Tong et al. [18] investigated a 2D axisymmetric numerical model of metal hydride tank packed with LaNi<sub>5</sub> and heated with phase change material (PCM) on Comsol platform, this model was validated by comparing the simulation results with the experiment data from other work. The Metal foam (MF) is composited into PCM to increase effective thermal

conductivity. The results shown improved heat transfer and hydrogen storage efficiency. Copper foam shows better performance of system than that with aluminium.

In [19], the authors carried out a comparative study between three different cooling system ( natural convection, finned heat pipe and a heat pipe on the central axis). They found that finned heat pipe has a significant effect on the hydrogen charge time, which reduced by approximately 75% at 10 bar hydrogen supply pressure.

In the present work, we investigate an integrated system based on a thermal coupling of a PEMFC and a metal hydride tank. In this system, the FeTi tank is heated through convection by a PEMFC operating at a typical 500 W electrical power. We study the energy balance between the PEMFC and the storage system. A heat exchanger is used to supervise the heat exchanging between the PEM fuel cell stack and the metal hydride tank. We derive the analytical expressions for the thermal power produced during PEMFC operation and the corresponding thermal power required for hydrogen desorption from the tank as a function of the mass flow rate, the operating temperature of the fuel cell, and the MH enthalpy of desorption. Based on these calculations, we develop a mathematical model that accounts for heat transfer in the integrated system, as well as mass transfer and desorption kinetics in the tanks, and solve for the dynamics of the coupled system at typical operating conditions. This paper is organized as follows: Section 2 consists of describing the energy management system. In section 3, we detail the control system. Section 4 presents the simulation results and a discussion, and section 5 presents a general conclusion.

## 2. Energy management

### 2.1. System modelling

A typical architecture of a benchmark system used in a hybrid electric vehicle is illustrated in Fig 1. The system includes a metal hydride tank, a PEM fuel cell, a pump, a heat exchanger, a flow meter, a valve and a servomotor. This system allows for the study of the thermal coupling of a PEM fuel cell and a metal hydride tank. The operation of this coupling consists of using the heat exchanger to supervise the heat exchanging between the PEM fuel cell stack and the metal hydride tank. In this topology, the transmitting calories produced by the fuel cell to the hydride tank is made by the circulation of a liquid cooling through a heat exchanger.

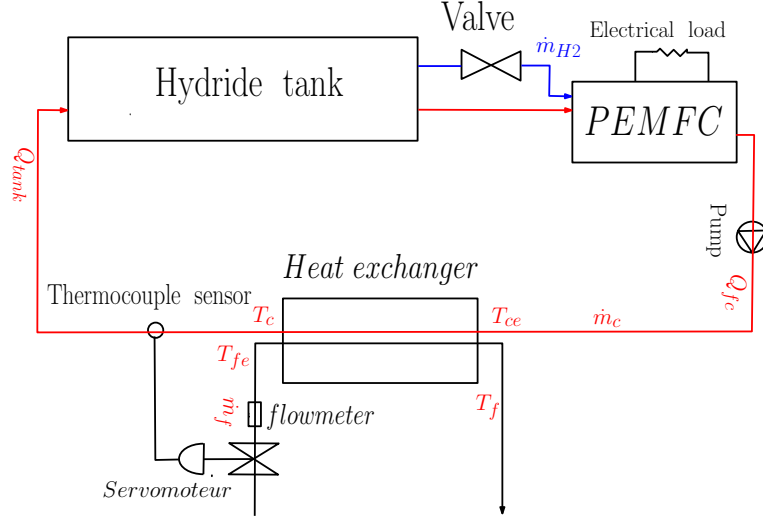


Figure 1: Synoptic schema of system

## 2.2. PEMFC modelling

The primary objective of modelling the fuel cell is to calculate the amount of heat produced by the stack at any operating point. The cell voltage of a PEM fuel cell ( $V_{cell}$ ) can be represented by a polarization curve, which can be calculated as shown in the following equation (1) by calculating the Nernst equations ( $E_{nernst}$ ) and the losses including activation losses  $V_{act}$ , ohmic losses  $V_{ohm}$ , and mass transport losses,  $V_{con}$  [20, 21]. Each of these losses affects the cell voltage at different region in the polarization curve [22].

The cell voltage at different region in the polarization curve.

$$V_{cell} = E_{nernst} - V_{act} - V_{ohm} - V_{con} \quad (1)$$

The Nernst equation represents the open circuit voltage  $E_{nernst}$  which is governed by a chemical potential

$$E_{nernst} = 1.229 - 0.000845(T_{fc} - 298.15) + 0.000431 T_{fc} \ln(P_{H_2} P_{O_2}^{0.5}) \quad (2)$$

where  $P_{O_2}$  and  $P_{H_2}$  are the partial pressures at the cathode and the anode respectively.  $T_{fc}$  is the temperature of the fuel cell. The two pressures are calculated as a function of the load current ( $i_{fc}$ ) and the temperature of the fuel cell.

$$P_{O_2} = \frac{P_{ca}}{\exp\left(\frac{1.636 i_{fc}}{T_{fc}^{1.334}}\right)} - P_{H_2O}^{sat} \quad (3)$$

$$P_{H_2} = 0.5 \frac{P_{an}}{\exp\left(\frac{1.636 i_{fc}}{T_{fc}^{1.334}}\right)} - P_{H_2O}^{sat} \quad (4)$$

$P_{H_2O}^{sat}$  is the saturation pressure which is a function of the temperature of the fuel cell [23], given in the following equation:

$$\log_{10}(P_{H_2O}^{sat}) = - 1.69 \cdot 10^{-10} T_{fc}^4 + 3.85 \cdot 10^{-7} T_{fc}^3 - 3.39 \cdot 10^{-4} T_{fc}^2 + 0.143 T_{fc} - 20.92 \quad (5)$$

According to Tafel equation, the activation loss can be expressed as follows [21]:

$$V_{ohm} = i_{fc} R_{ohm} \quad (6)$$

$$V_{con} = i_{fc} \left( a \frac{i_{fc}}{i_{lim}} \right)^b \quad (7)$$

The parameters "a" and "b" are computed by a nonlinear regression proposed by Pukrushpan et al [23]

### 2.3. Hydride tank modelling

The metal hydride bed is considered as a uniform mixture of a solid porous phase and a gaseous phase. This model incorporates the heat and mass balances that are applied to both metal hydride and hydrogen gas within the tank, considering the heat transfer from an external circulating water channel with a heat transfer coefficient assumed constant. This model was validated in our previous work [24]

To simplify the model, the following assumptions are considered:

- The gas phase is ideal, from a thermodynamic point of view;
- The media are in local thermal equilibrium between gas and solid;
- The solid phase is isotropic and has a uniform and constant porosity;
- The radiative transfer in the porous medium are neglected;
- The reactor is considered in two dimensions;

#### 2.3.1. Mass balance

The hydrogen concentration distribution in the MH bed and its evolution as a function of time is given by the mass balance law which is expressed as follows:

for the gas.

$$\epsilon \frac{\partial \rho_g}{\partial t} = -n_d - \dot{m}_{H_{2out}} \quad (8)$$

where  $\dot{m}_{H_{2out}}$  is the mass flow demand for a fuel cell which is given as following :

$$\dot{m}_{H_{2out}} = \frac{M_{H_2} P_{fc}}{2F V_{fc}} \quad (9)$$

where  $P_{fc}$  is the electrical power given by the following equation:

$$P_{fc} = N I_{fc} V_{cell} \quad (10)$$

Assuming the solid volume is fixed, the mass balance for the solid is:

$$(1 - \epsilon) \frac{\partial \rho_s}{\partial t} = n_d \quad (11)$$

### 2.3.2. Kinetic reaction

The hydrogen mass desorbed per unit time and unit volume,  $n_d$ , is given by the following expression:

$$n_d = C_d \left( \frac{-E_d}{RT} \right) \left( \frac{P_g - P_{eq}}{P_{eq}} \right) (\rho_s - \rho_0) \quad (12)$$

where  $P_{eq}$  is the equilibrium pressure that is given as a function of the temperature of the and the hydrogen-to-metal atomic ratio (HM). It is calculated using experimental data as follows:

$$P_{eq} = f (wt\%) \exp \left( -\frac{|\Delta H|}{R} \left( \frac{1}{T} - \frac{1}{T_{ref}} \right) \right) \quad (13)$$

where  $f (wt\%)$  is the equilibrium pressure at the reference temperature  $T_{ref}$ . This function is given by fitting the experimental data of the PCT curve (Figure 2) that has been obtained by Chabane et al in [25].

The hydrogen concentration in the solid is given as follows:

$$wt\% = \frac{m_{H_2}}{m_M + m_{H_2}} 100 \quad (14)$$

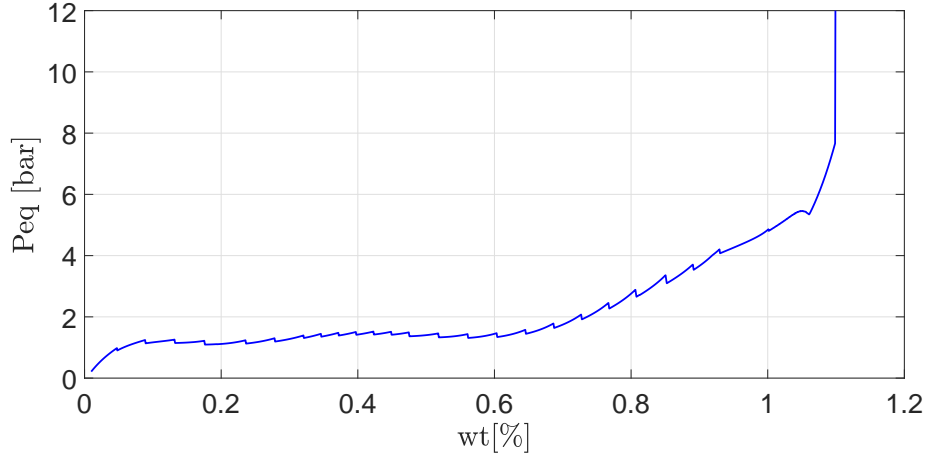


Figure 2: PCT curve of  $FeTi$  at  $21^{\circ}C$

The best fitting is obtained with a polynomial function of order 7. The coefficients of this polynomial for the desorption case are given in Table 1.

$$f(wt) = \sum_{i=0}^{n=7} a_i (wt\%)^i \quad (15)$$

Table 1: Polynomial function of equilibrium pressure

	$a_0$	$a_1$	$a_2$	$a_3$
$10^3$	-0.001	0.0386	-0.388	1.8642
	$a_4$	$a_5$	$a_6$	$a_7$
$10^3$	-4.6387	6.14	-4.0849	1.0748

#### 2.4. The heater modelling

Hydrogen molecule extraction from interstitial sites requires heat in order to split the chemical bonds between the hydrogen and the atom of the alloy and therefore supply the fuel cell by hydrogen. The thermal power produced by the cell can be used to maintain the hydride at equilibrium conditions (pressure and temperature) and therefore ensures the continuity of the desorption reaction. The thermal management of a PEM fuel cell coupled to a metal hydrogen storage system is carried out by thermal bridging (heat exchanger) between the two sources. In the current work, the choice of exchanger technology used to achieve the thermal bridge is counter-current heat exchanger. This choice of this technology is justified as follows:

- The temperature differences for this technology are almost constant (uniform) along the heat exchanger



- The exchange coefficient is substantially greater than that of a co-current exchanger, which promotes heat exchange.

In order to model the heat exchanger, we consider the following assumptions:

- No heat loss, the separation surface is the only exchange surface;
- The physical properties of the two fluids are constant;
- The transfer coefficient  $h$  is constant in the exchanger;
- The two heat transfer fluids are of the same nature.

By carrying out a heat balance, the heat flow exchanged between the hot and cold fluids and the temperatures at the outlet of the heat exchanger are determined by the following equation:

$$\begin{cases} m_f C_{p_f} \frac{dT_f}{dt} = \dot{m}_f C_{p_f} (T_{fe} - T_f) + hA (T_c - T_f) \\ m_c C_{p_c} \frac{dT_c}{dt} = \dot{m}_c C_{p_c} (T_{ce} - T_c) - hA (T_c - T_f) \end{cases} \quad (16)$$

Where :

- $m_f, m_c$  are respectively the masses of the cold fluid and the hot fluid [ $kg$ ].
- $C_{p_f}, C_{p_c}$  are respectively the heat capacities of cold and hot fluids [ $J/kg/K$ ];
- $T_{fe}, T_{ce}$  are the input temperatures of the cold and hot circuits [ $K$ ];
- $T_f, T_c$  are respectively the output temperatures of the cold and hot circuits [ $K$ ];
- $\dot{m}_f, \dot{m}_c$  are the mass flow rates of the cold and hot circuits [ $kg/s$ ];
- $A$  is the heat exchange surface [ $m^2$ ];
- $h$  is the heat transfer coefficient [ $W/m^2/K$ ].

According to equation ((16)) the heat exchanger is nonlinear, therefore, using a linear control will lead to ineffective control. The objective of this section is to accurately model a heat exchanger loop and to use this model to develop a linear control law with a minimum number of tuning parameters.

$$\begin{aligned} \dot{x}_1 &= c_1 * T_{ce} - c1 * x_1 - c_2 * K_e * A * (x_1 - x_2) \\ \dot{x}_2 &= c_3 * T_{fe} * u - c_3 * u * x_2 + c4 * K_e * A * (x_1 - x_2) \end{aligned} \quad (17)$$

Where  $x_1$  is the output temperature of the hot circuit (primary circuit),  $x_2$  is the output temperature of the cold circuit (secondary circuit). The  $u$  command is the cold circuit

flow and  $T_{ce}$  is the PEMFC output temperature which is considered to be the disturbance.  $c_1 \dots c_4$ ,  $K_e$  and  $A$  are the system parameters defined as follows :

$$\begin{aligned}
 c_1 &= \frac{\dot{m}_c}{m_c} & c_2 &= \frac{1}{m_c C_p} \\
 c_3 &= \frac{1}{m_f} & c_4 &= \frac{1}{m_f C_p} \\
 K_e &= \text{heat exchange coefficient} & A &= \text{exchange area [m}^2\text{]}
 \end{aligned}$$

In order to determine a linear model of this heat exchanger, the following steps should be considered:

- Determination of the points of equilibrium;
- Definition of the state space model;
- Modelling in the Laplace domain (open loop transfer function).

Before linearizing the model to find the state space, we compute the values of state variables in the steady state. The operating point is  $T_c = 21^\circ C$ . The values of the stationary states are defined by simulation. The equilibrium points are:

$$\begin{aligned}
 x_1 &= 294.153 [K] \\
 x_2 &= 286.42 [K]
 \end{aligned}$$

The linearization of a non-linear system around an operating point is obtained by estimating the Jacobian at equilibrium points. Let the following be a non-linear system:

$$\begin{aligned}
 \dot{x} &= f(x, u) \\
 y &= g(x, u)
 \end{aligned} \tag{18}$$

where:

$\dot{x}$ : is the variation of the two temperatures at the exit of the heat exchanger;  
 $y$  is the thermal power exchanged between the two heat transfer circuits of the heat exchanger.

With this linearization around a rest point, the system can be described by the following linear state mathematical model:

$$\begin{aligned}
 \dot{x} &= Ax + Bu \\
 y &= Cx + Du
 \end{aligned} \tag{19}$$

where " $x$ " is a measurable system state vector, " $y$ " is the system output, " $u$ " is the control input, " $A$ " is the drift dynamic of the system, " $B$ " is the input matrix, " $C$ " is the

output matrix and "D" is the action direct matrix [26].

$$A = \left( \begin{array}{cccc} \frac{\partial f_1}{\partial x_1}(x) & \frac{\partial f_1}{\partial x_2}(x) & \cdots & \frac{\partial f_1}{\partial x_n}(x) \\ \frac{\partial f_2}{\partial x_1}(x) & \ddots & & \vdots \\ \vdots & & \ddots & \vdots \\ \frac{\partial f_n}{\partial x_1}(x) & \cdots & \cdots & \frac{\partial f_n}{\partial x_n}(x) \end{array} \right)_{|x=x_0}$$

$$B = \left( \begin{array}{cccc} \frac{\partial g_1}{\partial x_1}(x) & \frac{\partial g_1}{\partial x_2}(x) & \cdots & \frac{\partial g_1}{\partial x_m}(x) \\ \frac{\partial g_2}{\partial x_1}(x) & \ddots & & \vdots \\ \vdots & & \ddots & \vdots \\ \frac{\partial g_m}{\partial x_1}(x) & \cdots & \cdots & \frac{\partial g_m}{\partial x_m}(x) \end{array} \right)_{|x=x_0}$$

$$C = \left( \begin{array}{c} \frac{\partial g_1}{\partial u}(x) \\ \frac{\partial g_2}{\partial u}(x) \\ \vdots \\ \frac{\partial g_m}{\partial u}(x) \end{array} \right)_{|x=x_0; u=u_0}$$

the linearization of this model gives :

$$A = \begin{bmatrix} -0.008258000848966308 & 0.002702445293410753 \\ 2.152485299411193e-7 & -0.4000002152485299 \end{bmatrix}$$

$$B = \begin{bmatrix} 0 \\ -0.3503333333333387 \end{bmatrix}$$

$$C = [ 33.929200658772 \quad -33.929200658772 ]$$

$$D = [0]$$

The open-loop transfer function, ( $G(s)$ ), describing the relationship between the flow rate of the secondary circuit of the exchanger and the amount of calories exchanged for a constant flow rate of the primary circuit is obtained as follows:

$$G(s) = \frac{20.46s + 0.06818}{s^2 + 0.01411s + 4.0109e^{-5}} \quad (20)$$

The stability of the system is verified by calculating the eigenvalues of the matrix A, these parameters are found to be:

$$\lambda_1 = -0.0083 \quad \lambda_2 = -0.4$$

The poles of the open loop transfer function (FTBO, the two eigenvalues of the matrix A) are all real and negative. Moreover, the order of the polynomial in the numerator is lower than that of the denominator in each case, therefore, the obtained model is stable.

### 2.5. Components modelling

In this section we summarize the models of the components used to achieve the thermal coupling.

- Valve :

$$H_v(s) = \frac{3}{0.5s + 1} \quad (21)$$

- Servomotor :

$$H_{sm}(s) = \frac{0.314}{(0.2s + 1)^2} \quad (22)$$

- Flowmeter :

$$H_{deb}(s) = \frac{3}{0.01s^2 + 0.0047s + 1} \quad (23)$$

Therefore, the open loop transfer function of the flow control is:

$$H(s) = \frac{0.942}{0.0002s^5 + 0.002494s^4 + 0.03013s^3 + 0.2542s^2 + 0.9047s + 1} \quad (24)$$

### 2.6. Energy balance

The thermal power to be supplied to the hydride reservoir during the desorption is proportional to the hydrogen flow required by the FC, which depends on the electric charge current. This is the maximal power given as follows:

$$Q = \dot{m}_{H_2} \frac{\Delta H}{M_{H_2}} \quad (25)$$

As a function of the current of the fuel, cell, this power can be written as follows:

$$Q = \frac{N_{cell} I_{pac} * M_{H_2}}{2F} \Delta H \quad (26)$$

with :

- $\dot{m}_{H_2}$ : is the mass flow rate [ $kg/s$ ];
- $\Delta H$ : is the enthalpy of formation [ $J/kg$ ];
- $M_{H_2}$ : is the molar mass of hydrogen [ $kg/mol$ ];

- $F$ : is the Faraday constant;
- $N_{cell}$ : is the number of cells ;
- $I_{pac}$ : is the load current;

The heat produced by the fuel cell is calculated as follows:

$$Q_{fc} = I N (1.45 - V_{cell}) \quad (27)$$

The power exchanged between the fuel cell and the heat transport is given by the following equation 28:

$$Q_{H2O} = \dot{m}_{H2O} C_{pH2O} (T_{out} - T_{in}) \quad (28)$$

Assuming that all the heat produced by the cell is transmitted into the heat transport circuit, the temperature of the cell is given by:

$$T_{pac} = T_{pac_{in}} + \frac{Q_{pac}}{\dot{m}_{H2O} C_p} \quad (29)$$

where:

- $\dot{m}_{H2O}$ : is the mass flow rate of the cooling circuit [ $kg/s$ ];
- $C_{pH2O}$ : is the heat capacity of water [ $J/kg/K$ ];
- $T_{output}$  and  $T_{input}$ : are respectively the input and output temperatures of the internal heat transfer circuit of the FC [ $K$ ];
- $V_{cell}$ : is the voltage of a cell in the stack of FC [ $V$ ].

By performing a power balance between the power produced by the PEMFC and the power required during the desorption for a battery consumption profile (Figure 1), the amount of heat that the cooling system must evacuate and the temperature at the tank inlet are:

$$Q_{ech} = Q_{pac} - Q_{MH} \quad (30)$$

$$T_{Tank_{in}} = T_{pac} - \frac{Q_{ech}}{\dot{m}_{H2O} C_p} \quad (31)$$

### 3. System control

As discussed, the studied system consists of a heat exchanger, supplied with two actuators and three sensors:

- a valve for the secondary circuit of the exchanger whose characteristics are a gain in flow  $K_v = 3 [l/s/rad]$  and a time constant  $\tau_v = 0.5 [s]$ .
- a servomotor for controlling the water intake valve, consisting of an electromechanical system whose transfer function between the control voltage and the output angle is characterized by a gain in the position  $G = \pi/10 [rad/V]$  and a time constant  $T = 0.2 [s]$ .
- a flow meter for measuring the flow of water flowing in the secondary circuit of the exchanger.

The PI controller (Proportional Integral) is known for its simplicity of design and implementation. However, due to the strong nonlinear character of the system (heat exchanger), it is necessary to linearize the system around an operating point before reaching the functional control scheme given in Figure 3.

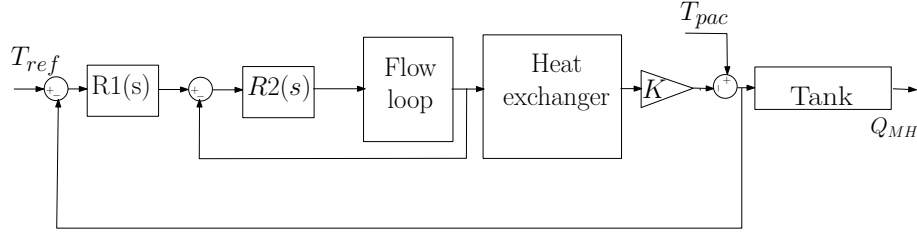


Figure 3: Closed-loop system representation

The characteristics of this block diagram are:

- $T_{ref}$  is the inlet temperature of the tank  $[K]$ , which is fixed to  $21^{\circ}C$ . This value corresponds to the experimental value.
- $T_{pac}$  is the temperature of fuel cell  $[K]$ ;
- $Q_{MH}$  is the thermal power supplied to the hydride by the heat transfer circuit  $[Watt]$ .

The input to regulator  $R2(s)$  is the output signal of regulator  $R1(s)$ . The output of  $R2(s)$  supplies the control variable which acts on the servomotor for controlling the intake valve of the secondary circuit of the heat exchanger. This is done by controlling the opening angle of the valve. The output quantity of the exchanger is the heat flux exchanged between the two circuits (hot/cold). The cold circuit makes it possible to calculate the exit temperature of the exchanger as a function of the flow of the circuit.

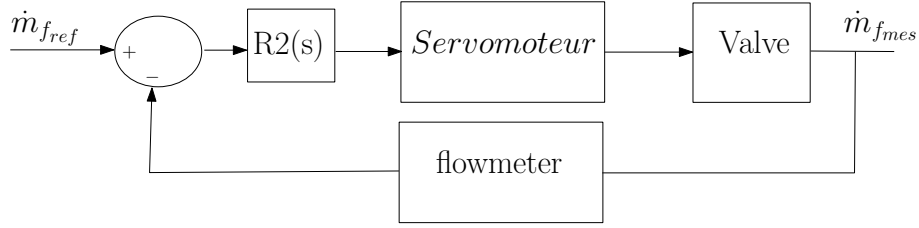


Figure 4: Closed-loop Control of mass flow

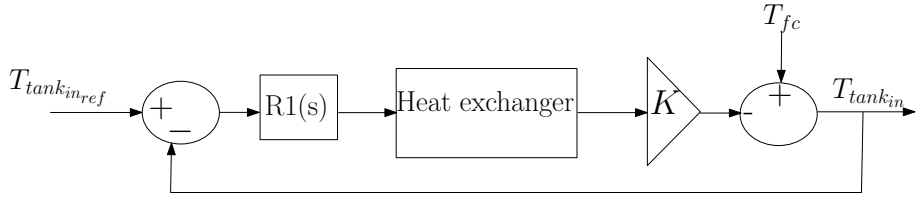


Figure 5: Closed-loop Control of water temperature

The open-loop transfer function,  $H(s)$ , of the flow control is equal to the product of the different transfer functions of the components constituting the direct chain (servomotor, valve and flowmeter). PID (Proportional Integral Derivative) controllers are sufficient to solve a large number of control problems, especially for systems that are characterized by slow dynamics. Several methods are reported in the literature for the parameterization of PID correctors, including the Test-Error Method [ref], the Ziegler and Nichols Method [ref] and the Cohen and Coon Method [27–31]. These methods are widely used in the industry. Another method rarely used, the Magnitude Optimum (MO) technique, provides a non-oscillatory, closed-loop response for a large class of process models. However, this technique is based on a transfer function model that requires precise identification of processes and in-depth calculations.

Suppose that the present process can be described by the following rational transfer function:

$$G_p(s) = K_{pr} \frac{1 + b_1s + b_2s^2 + \dots + b_ms^m}{1 + a_1s + a_2s^2 + \dots + a_ns^n} e^{-sT_{del}} \quad (32)$$

where  $K_{pr}$  is the static gain,  $a_i$  and  $b_i$  are the parameters of the transfer function ( $m \leq n$ ) and  $T_{del}$  is the pure delay of the system. The PID corrector is described by the following transfer function:

$$G_c(s) = \frac{K_i}{s} + K + \frac{sK_d}{1 + sT_f} \quad (33)$$

Where  $K_i$ ,  $K$ ,  $K_d$  and  $T_f$  represent integral gain, proportional gain, derivative gain, and filter time constant. The main goal of this method is to find parameters that meet a criterion that has a closed-loop system amplitude response,  $G_{bf}$ , closer to 1 over a wide bandwidth. This requirement can be expressed as follows:

$$|G_{bf}| = \left| \frac{G_p(s)G_c(s)}{1 + G_p(s)G_c(s)} \right| \approx 1 \quad (34)$$

In order to calculate the parameters of the PID according to the MO criterion, Varonique et al in [26] propose to put the transfer function  $G_{bo}$  in a polynomial form using the development of Taylor which is expressed as follows:

$$G_{bo} = A_0 - A_1s + A_2s^2 - A_3s^3 + \dots \quad (35)$$

Where  $A_i(1, 2 \dots k)$  are the integrals of the impulse response of the system that are determined using the repetitive integration method [26] as follows:

$$\begin{aligned} A_0 &= K_{pr} \\ A_1 &= K_{pr}(a_1 - b_1 + T_{del}) \\ A_2 &= K_{pr} \left[ b_2 - a_2 - T_{del}b_1 + \frac{T_{del}^2}{2!} \right] + A_1a_1 \\ &\vdots \\ A_k &= K_{pr} \left[ (-1)^{k+1}(a_k - bk) + \sum_{i=1}^k (-1)^{k+1} \frac{T_{del}^i b_{k-1}}{i!} \right] + \sum_{i=1}^{k-1} (-1)^{k+i-1} A_i a_{k-i} \end{aligned} \quad (36)$$

$$\begin{bmatrix} K_i \\ K \\ K_d \end{bmatrix} = \begin{bmatrix} -A_1 & A_0 & 0 \\ -A_3 & A_2 & -A_3 - T_f A_0 \\ -A_5 & A_4 & -A_3 - T_f A_2 - T_f^2 A_1 - T_f^3 A_0 \end{bmatrix}^{-1} \times \begin{bmatrix} -0.5 \\ 0 \\ 0 \end{bmatrix} \quad (37)$$

In our case, there is no pure delay,  $T_{del} = 0$  and  $T_f$  is the filter time constant which is expressed as follows:

$$T_f = \frac{K_d}{K N} \quad (38)$$

The value of  $T_f$  is determined by solving the following equation [26]:

$$T_f^4 N A_0 A_3 + T_f^3 N A_1 A_3 + T_f^2 N (A_2 A_3 - A_0 A_5) + T_f N (A_3^2 - A_1 A_5) + A_2 A_5 - A_3 A_4 = 0 \quad (39)$$

The value of  $N$  is typically between 8 and 20 according to [32].

The following method is used to determine the parameters of the two regulators: the controller of the mass flow

$$\begin{bmatrix} K_i \\ K \\ K_d \\ T_f \end{bmatrix} = \begin{bmatrix} 0.347 \\ 0.162 \\ 0.0551 \\ 0.703 \end{bmatrix} \quad (40)$$



the controller of the heater :

$$\begin{bmatrix} K_i \\ K \\ K_d \\ T_f \end{bmatrix} = \begin{bmatrix} -0.00146 \\ -0.167 \\ 0.0558 \\ 0.369 \end{bmatrix} \quad (41)$$

#### 4. Simulation and discussion

The inlet temperature of the heat transfer circuit is used as a reference for controlling the flow rate of the cold circuit of the exchanger. Driven by the servomotor, the valve will regulate the flow of the secondary circuit of the exchanger which will condition the heat exchange and the input temperature of the hot circuit in the tank. The simulation block diagram is executed in MATLAB/Simulink, depicted in Figure 6.

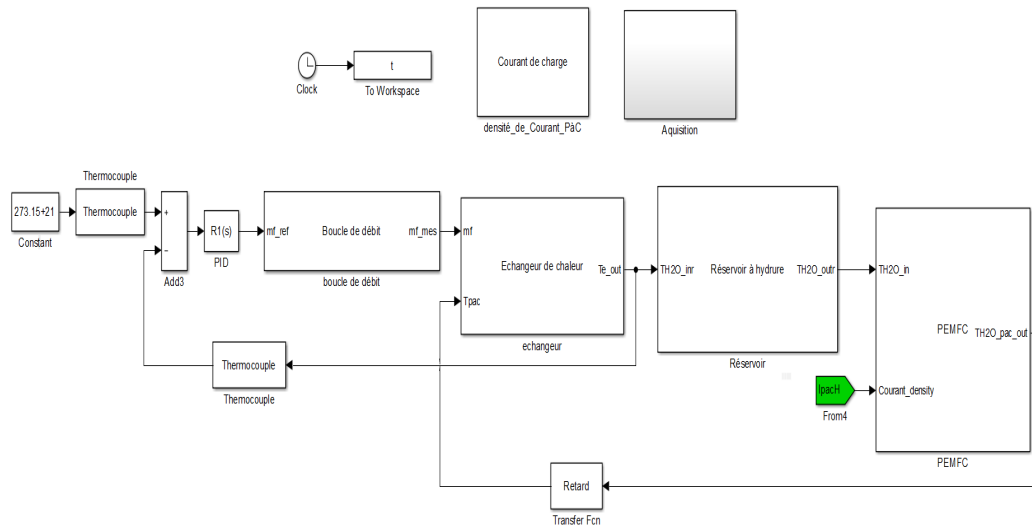


Figure 6: Simulink model of the thermal coupling of fuel cell and metal hydride tank.

Figure 7 illustrates the PEMFC demand for hydrogen flow corresponding to the profile used to supply the fuel cell.

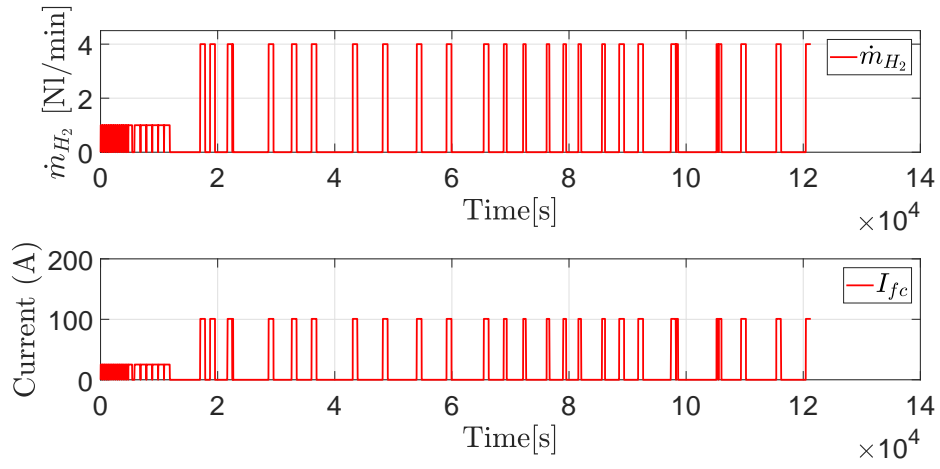


Figure 7: Profil Of hydrogen mass flow

The response of the system is illustrated in the figures 8 and 9.

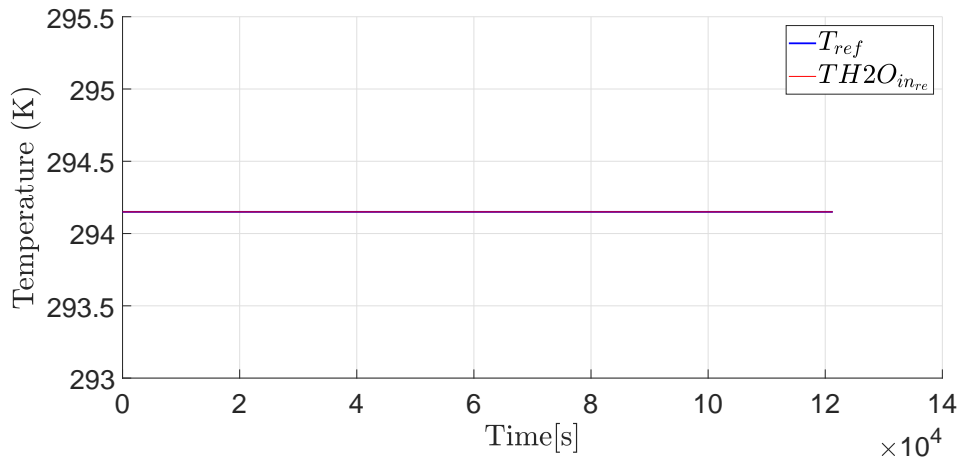


Figure 8: Water temperature variation vs.time

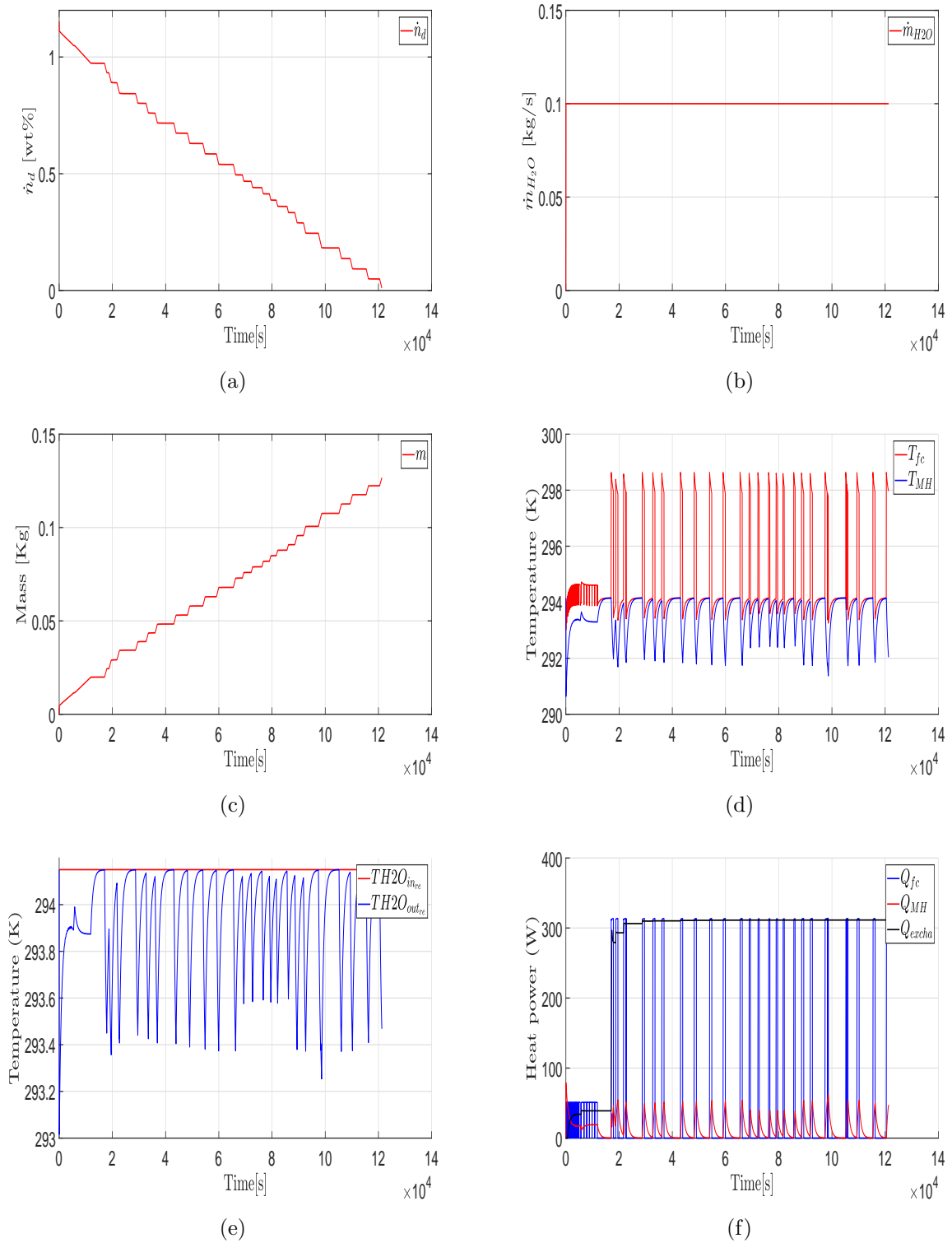


Figure 9: Simulation results

Figure 9(a) depicts the time-dependent changes of hydrogen to metal (H/M) ratio. At the beginning, the hydrogen discharge rate of the tank drops without the addition of heat to the hydride tank. This is due to the presence of gaseous hydrogen present. During this phase, the temperature of the metal bed decreases abruptly, followed by an increase to reach the equilibrium temperature, as shown in figure (9(d)). The full discharge time occurs at 31 h. It can be also be observed that the total hydrogen capacity (which is 1.18 wt %) stored in the tank was desorbed.

The mass of the hydrogen extracted from the hydride is inversely proportional to the desorption kinetic (9(c)). The total mass of hydrogen released from the hydride is about 145 g.

As shown in figure9(d), the operating temperature of the PEMFC is never reached because of the direct coupling of the battery to the tank (same heat transport circuit). It can be seen that the coolant circuit limits the evolution of the temperature of the FC towards its operating temperature ( $65^{\circ}C$ ), because it is cooled in a constant manner by the temperature of the cooling circuit at the outlet of the tank. The temperature of the outlet of the tank is always less than  $21^{\circ}C$ , thus making the evolution of the temperature of the stack very limited. In this topology, the control carried out does not allow for the control of the temperature of the FC, thus affecting the energy efficiency of the two sources. In order to maintain the operating temperature of FC, another topology of heat exchange management is studied in the next section.

Figure 9(e) shows the time evolution of the temperature at the inlet and the outlet of the heat transfer circuit of the internal exchanger of the tank. As can be seen, only the temperature at the exit varies with time and it depends on hydrogen flow rate required by the fuel cell. This induces a variation of the amount of hydrogen in the tank, thus generating a fall in temperature which will in turn gradually increase towards the inlet temperature.

The various thermal powers implicated in this coupling between the different sources are reported on the Figure 9(f). The heat consumed by the FeTi alloy to desorb the hydrogen at the hydrogen mass flow required by the fuel cell is about  $65[Watt]$ , where the power produced by the fuel cell is about  $330 [Watt]$ . As suggested by figure 9(f), only about 20% of the total heat produced by the fuel cell should be transferred to MH tank using the heat exchanger to maintain the temperature of the tank at  $21^{\circ}C$ . The excess of the power produced is removed to the secondary circuit of the heat exchanger, which is represented in figure 9(f) by the black line.

## 5. conclusion

In this work, we investigate a thermal coupling potential between a FeTi alloy tank and a PEM fuel cell, using a heat transfer fluid to manage the thermal exchanges between these two sources in order to maintain hydrogen desorption at a constant temperature. The remaining thermal power is then transmitted to the environment by a secondary circuit of

the exchanger, using an appropriately adjusted excess of water rate. We propose a generic physical model that accounts for heat transfer in all the components of the integrated system (fuel cell, metal hydride tank and tubular exchanger), as well as hydrogen desorption kinetics and flow in the tank. Based on this model, we study the dynamics of the coupled storage/usage system in terms of the hydrogen pressure in the tank, and the temperatures in the tank and the fuel cell. The simulation results showed that the FC efficiently covers the required power of the reservoir. The series coupling induces a limitation of the evolution of the temperature of the FC: the operating temperature of the FC is never reached. For this type of configuration, the temperature of the hydride imposes the thermal behaviour of the fuel cell.

## References

- [1] B. D. MacDonald, A. M. Rowe, A thermally coupled metal hydride hydrogen storage and fuel cell system, *Journal of Power Sources* 161 (1) (2006) 346–355. doi:10.1016/j.jpowsour.2006.04.018.  
URL <https://www.sciencedirect.com/science/article/pii/S0378775304010742>
- [2] B. D. MacDonald, A. M. Rowe, A thermally coupled metal hydride hydrogen storage and fuel cell system, *Journal of Power Sources* 161 (1) (2006) 346–355. doi:10.1016/j.jpowsour.2006.04.018.  
URL <https://www.sciencedirect.com/science/article/pii/S0378775306006586>
- [3] P. Pfeifer, C. Wall, O. Jensen, H. Hahn, M. Fichtner, Thermal coupling of a high temperature PEM fuel cell with a complex hydride tank, *International Journal of Hydrogen Energy* 34 (8) (2009) 3457–3466. doi:10.1016/j.ijhydene.2009.02.041.  
URL <https://www.sciencedirect.com/science/article/pii/S0360319909002754>
- [4] J. Fernández-Moreno, G. Guelbenzu, A. Martín, M. Folgado, P. Ferreira-Aparicio, A. Chaparro, A portable system powered with hydrogen and one single air-breathing PEM fuel cell, *Applied Energy* 109 (2013) 60–66. doi:10.1016/J.APENERGY.2013.03.076.  
URL <https://www.sciencedirect.com/science/article/pii/S0306261913002729>
- [5] H. S. Han, C. Cho, S. Y. Kim, J. M. Hyun, Performance evaluation of a polymer electrolyte membrane fuel cell system for powering portable freezer, *Applied Energy* 105 (2013) 125–137. doi:10.1016/J.APENERGY.2012.12.056.  
URL <https://www.sciencedirect.com/science/article/pii/S0306261912009476>
- [6] B. Delhomme, A. Lanzini, G. A. Ortigoza-Villalba, S. Nachev, P. De Rango, M. Santarelli, P. Marty, P. Leone, Coupling and thermal integration of a solid oxide fuel cell with a magnesium hydride tank, *International Journal of Hydrogen Energy* 38 (11) (2013) 4740–4747. doi:10.1016/j.ijhydene.2013.01.140.  
URL <https://www.sciencedirect.com/science/article/pii/S0360319913002498>
- [7] S. H. Kim, C. M. Miesse, H. B. Lee, I. W. Chang, Y. S. Hwang, J. H. Jang, S. W. Cha, Ultra compact direct hydrogen fuel cell prototype using a metal hydride hydrogen storage tank for a mobile phone, *Applied Energy* 134 (2014) 382–391. doi:10.1016/J.APENERGY.2014.08.019.  
URL <https://www.sciencedirect.com/science/article/pii/S0306261914008228>
- [8] A. G. Yiotis, M. E. Kainourgiakis, L. I. Kosmidis, G. C. Charalambopoulou, A. K. Stubos, Thermal coupling potential of Solid Oxide Fuel Cells with metal hydride tanks: Thermodynamic and design considerations towards integrated systems, *Journal of Power Sources* 269 (2014) 440–450. doi:10.1016/j.jpowsour.2014.07.023.  
URL <https://www.sciencedirect.com/science/article/pii/S0378775314010660>
- [9] Z. Liu, Y. Li, Q. Bu, C. J. Guzy, Q. Li, W. Chen, C. Wang, Novel fuel cell stack with coupled metal hydride containers, *Journal of Power Sources* 328 (2016) 329–335. doi:10.1016/j.jpowsour.2016.07.096.  
URL <https://www.sciencedirect.com/science/article/pii/S0378775316309715>
- [10] A. P. Tetuko, B. Shabani, J. Andrews, Thermal coupling of PEM fuel cell and metal hydride hydrogen storage using heat pipes, *International Journal of Hydrogen Energy* 41 (7) (2016) 4264–4277.

- doi:10.1016/j.ijhydene.2015.12.194.  
 URL <https://www.sciencedirect.com/science/article/pii/S0360319915313501>
- [11] M. V. Lototskyy, I. Tolj, L. Pickering, C. Sita, F. Barbir, V. Yartys, The use of metal hydrides in fuel cell applications, *Progress in Natural Science: Materials International* 27 (1) (2017) 3–20. doi:10.1016/j.pnsc.2017.01.008.  
 URL <https://www.sciencedirect.com/science/article/pii/S1002007117300138>
- [12] V. Venkataraman, Thermal modelling and coupling of a heat pipe integrated desorber with a Solid Oxide Fuel Cell, *Applied Thermal Engineering* (2019) 943–961 doi:10.1016/j.applthermaleng.2018.10.131.  
 URL <https://www.sciencedirect.com/science/article/pii/S1359431118310603>
- [13] E. Harikishan Reddy, S. Jayanti, Thermal coupling studies of a high temperature proton exchange membrane fuel cell stack and a metal hydride hydrogen storage system, *Energy Procedia* 29 (2012) 254–264. doi:10.1016/j.egypro.2012.09.031.  
 URL <https://www.sciencedirect.com/science/article/pii/S1876610212014518>
- [14] J. Weiss-Ungethüm, I. Bürger, N. Schmidt, M. Linder, J. Kallo, Experimental investigation of a liquid cooled high temperature proton exchange membrane (HT-PEM) fuel cell coupled to a sodium alanate tank, *International Journal of Hydrogen Energy* 39 (11) (2014) 5931–5941. doi:10.1016/j.ijhydene.2014.01.127.  
 URL <https://www.sciencedirect.com/science/article/pii/S0360319914002079>
- [15] P. Rizzi, E. Pinatel, C. Luetto, P. Florian, A. Graizzaro, S. Gagliano, M. Baricco, Integration of a PEM fuel cell with a metal hydride tank for stationary applications, *Journal of Alloys and Compounds* 645 (S1) (2015) S338–S342. doi:10.1016/j.jallcom.2014.12.145.  
 URL <https://www.sciencedirect.com/science/article/pii/S0925838814030734>
- [16] M. Lototskyy, I. Tolj, Y. Klochko, M. W. Davids, D. Swanepoel, V. Linkov, Metal hydride hydrogen storage tank for fuel cell utility vehicles, *International Journal of Hydrogen Energy* (may 2019). doi:10.1016/j.ijhydene.2019.04.124.  
 URL <https://www.sciencedirect.com/science/article/abs/pii/S036031991931554X>
- [17] F. Askri, A. Miled, S. Mellouli, H. Ben Mâad, Numerical investigation of high temperature metal hydride water pumping system, *International Journal of Hydrogen Energy* 44 (31) (2019) 16777–16792. doi:10.1016/J.IJHYDENE.2019.04.263.  
 URL <https://www.sciencedirect.com/science/article/abs/pii/S0360319919317483>
- [18] L. Tong, J. Xiao, P. Bénard, R. Chahine, Thermal management of metal hydride hydrogen storage reservoir using phase change materials, *International Journal of Hydrogen Energy* 44 (38) (2019) 21055–21066. doi:10.1016/J.IJHYDENE.2019.03.127.  
 URL <https://www.sciencedirect.com/science/article/abs/pii/S0360319919311358>
- [19] F. A. Elhamshri, M. Kayfeci, Enhancement of hydrogen charging in metal hydride-based storage systems using heat pipe, *International Journal of Hydrogen Energy* 44 (34) (2019) 18927–18938. doi:10.1016/J.IJHYDENE.2018.10.040.  
 URL <https://www.sciencedirect.com/science/article/abs/pii/S0360319918332178>
- [20] F. Barbir, *PEM Fuel Cells : Theory and Practice* ACADEMIC PRESS, Academic Press, 2005.
- [21] J. Larminie, J. Lowry, *Electric Vehicle Technology Explained*, Wiley, 2012. doi:10.1002/9781118361146.  
 URL <https://www.wiley.com/en-us/Electric+Vehicle+Technology+Explained%2C+2nd+Edition-p-9781118361146>
- [22] A. Mohammadi, D. Chabane, G. Cirrincione, M. Cirrincione, A. Djerdir, Effect of the Temperature Distribution on the Performance of PEMFC Stacks for Fault Diagnosis, in: 2018 21st International Conference on Electrical Machines and Systems (ICEMS), IEEE, 2018, pp. 1019–1023. doi:10.23919/ICEMS.2018.8549518.  
 URL <https://ieeexplore.ieee.org/document/8549518/>
- [23] A. K. BILHAN, C. WANG, Control of Fuel Cell Power System, Vol. 6 of *Advances in Industrial Control*, Springer London, London, 2016. doi:10.17932/iau.ijemme.m.21460604.2016.6/3.1259-1265.  
 URL <http://link.springer.com/10.1007/978-1-4471-3792-4>
- [24] D. Chabane, F. Harel, A. Djerdir, D. Candusso, O. Elkedim, N. Fenineche, Energetic modeling, simulation and experimental of hydrogen desorption in a hydride tank, *International Journal of Hydrogen*

- Energy 44 (2) (2019) 1034–1046. doi:10.1016/j.ijhydene.2018.11.024.  
 URL <https://www.sciencedirect.com/science/article/pii/S0360319918335468>
- [25] D. Chabane, F. Harel, A. Djerdir, D. Candusso, O. ElKedim, N. Fenineche, A new method for the characterization of hydrides hydrogen tanks dedicated to automotive applications, *International Journal of Hydrogen Energy* 41 (27) (2016) 11682–11691. doi:10.1016/j.ijhydene.2015.12.048.  
 URL <https://www.sciencedirect.com/science/article/pii/S0360319915304146>
- [26] D. Vranči, S. Strmčnik, A. Juriči, A magnitude optimum multiple integration tuning method for filtered PID controller, *Automatica* 37 (9) (2001) 1473–1479. doi:10.1016/S0005-1098(01)00088-7.  
 URL <https://www.sciencedirect.com/science/article/pii/S0005109801000887>
- [27] E. D. E. Geest, Méthodes d'optimisation pour le réglage de contrôleurs PID, Tech. rep. (2001).
- [28] D. Fister, I. Fister, I. Fister, R. Šafarič, Parameter tuning of PID controller with reactive nature-inspired algorithms, *Robotics and Autonomous Systems* 84 (2016) 64–75. doi:10.1016/j.robot.2016.07.005.
- [29] M. B. Milovanović, D. S. Antić, M. T. Milojković, S. S. Nikolić, S. L. Perić, M. D. Spasić, Adaptive PID control based on orthogonal endocrine neural networks, *Neural Networks* 84 (2016) 80–90. doi:10.1016/j.neunet.2016.08.012.
- [30] H. Moradi, H. Setayesh, A. Alasty, PID-Fuzzy control of air handling units in the presence of uncertainty, *International Journal of Thermal Sciences* 109 (2016) 123–135. doi:10.1016/j.ijthermalsci.2016.05.024.  
 URL <https://www.sciencedirect.com/science/article/pii/S1290072916306573>
- [31] P. Shah, S. Agashe, Review of fractional PID controller, *Mechatronics* 38 (2016) 29–41. doi:10.1016/j.mechatronics.2016.06.005.  
 URL [www.elsevier.com/locate/mechatronics](http://www.elsevier.com/locate/mechatronics)
- [32] K. J. K. J. Astrom, T. Hagglund, *Advanced PID Control* - [Book Review], Vol. 26, ISA-The Instrumentation, Systems, and Automation Society, 2006. doi:10.1109/mcs.2006.1580160.  
 URL <https://www.passeidireto.com/arquivo/49913462/advanced-pid-control---karl-j-astrom-tore-hagglund>